Inorganic Chemistry

Article

pubs.acs.org/IC

Atom Transfer Radical Polymerization (ATRP) and Organometallic Mediated Radical Polymerization (OMRP) of Styrene Mediated by Diaminobis(phenolato)iron(II) Complexes: A DFT Study

Rinaldo Poli*[,†,‡] and Michael P. Shaver[§]

[†]CNRS, LCC (Laboratoire de Chimie de Coordination), 205 route de Narbonne, BP 44099, F-31077, Toulouse Cedex 4, France

[‡]Institut Universitaire de France, 103, bd Saint-Michel, 75005, Paris, France

[§]School of Chemistry, University of Edinburgh, West Mains Road, Edinburgh, EH9 3JJ, United Kingdom

Supporting Information

ABSTRACT: This study has addressed the radical polymerization of styrene mediated by the diaminobis(phenolate) complexes [Fe(O-2,4-$Y_2C_6H_2$-5-CH_2)$_2$N$CH_2CH_2NMe_2$], abbreviated as [Fe^{II}]. The system is known to be well controlled when Y = Cl but not when Y = alkyl. The control was proposed to occur by a dual ATRP+OMRP mechanism. We have used DFT calculations to address the Y = Cl and Y = CH_3 systems. The growing radical chain, ATRP dormant chain, and OMRP dormant chain were simplified to PhCH(CH_3)$^•$, PhCH(CH_3)-Cl, and [PhCH(CH_3)-Fe^{III}]. The idealized ATRP activation/deactivation equilibrium involves [Fe^{III}−Cl] (**I**^{Y}) and PhCH(CH_3)$^•$ on the active side and [Fe^{II}] (**II**^{Y}) and PhCH(CH_3)−Cl on the dormant side, whereas the OMRP activation/deactivation relates [Fe^{II}] and PhCH(CH_3)$^•$ with [PhCH(CH_3)-Fe^{III}] (**III**^{Y}). A benchmarking of various functionals against the known spin properties of alkylporphyriniron(III) shows B3PW91* to be a suitable functional. For the purpose of bond dissociation energy calculations, a dispersion correction was made (B3PW91*-D3). For both Y systems, the ground state is a spin sextet for **I**, a spin quintet for **II**, and a spin quartet for **III**. The calculations show a greater energy cost for the ATRP activation process involving Cl atom addition to **II**^{Cl} to yield **I**^{Cl} (7.2 kcal/mol) relative to the process transforming **II**^{Me} to **I**^{Me} (2.1 kcal/mol). On the other hand, the alkyl addition transforming **II** to **III** provides slightly greater stabilization for **II**^{Cl} (27.1 kcal/mol) than for **II**^{Me} (26.1 kcal/mol). As a result, both ATRP and OMRP trapping processes provide greater stabilization for the Y = Cl system, in agreement with the observed better control. The charge analysis attributes these minor but determining energy differences to the inductive electron withdrawing effect of the phenolato Cl substituents. The ATRP and OMRP activation/deactivation pathways have been analyzed in relation to the spin state change; they show in each case the absence of an activation barrier, and both processes corresponding to spin allowed single-state pathways occurring on the quartet (OMRP) and quintet (ATRP) potential energy surfaces. Molecular volume calculations suggest that the balance between ATRP and OMRP may shift in favor of the latter at higher pressures.

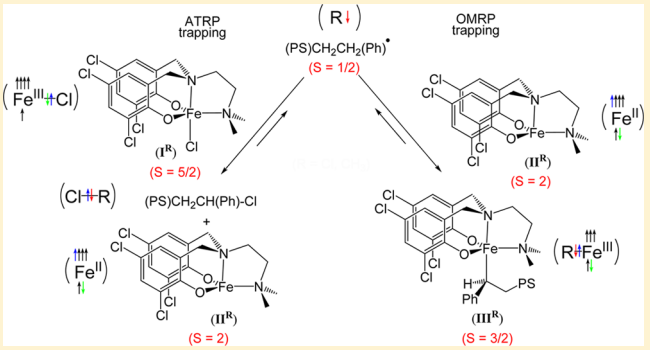

INTRODUCTION

Reversible deactivation radical polymerization (RDRP) is now a well established technique for the assembly of complex, precision-controlled, macromolecular architectures.[1] Numerous strategies exist for retarding the termination of growing macromolecular radicals, thereby prolonging the chain life and allowing the generation of materials with characteristics that approach those of ideal living polymers. Among these, atom transfer radical polymerization (ATRP) has emerged as one of the most general and robust methods. Inspired by the initial discovery of active Cu^I/Cu^{II}-X[2,3] and Ru^{II}/Ru^{III}-X[4,5] redox couples (X = halogen, typically Cl or Br), complexes of many other metals have been used to control an expansive monomer scope.[6,7] One of the challenges of this synthetic method is contamination of the isolated polymer by the metal complex. Although the metal complex exerts a catalytic function, namely it is not incorporated in the halogen chain-end functionalized polymer (Scheme 1), significant quantities of the potentially toxic or colored metal remain entrapped in the polymer, limiting its possible applications, particularly in the biomedical sector. Even though solutions exist for limiting the amount of catalyst down to the ppm level,[8] there has been interest in developing ATRP catalysts based on iron, which is an abundant, inexpensive, and especially biocompatible element.[9]

ATRP catalyzed by iron complexes was first introduced in 1997[10] and has since become a very active area of research. The

Received: April 21, 2014
Published: July 3, 2014

   dx.doi.org/10.1021/ic5009347 | Inorg. Chem. 2014, 53, 7580−7590

Scheme 1. Polymer Synthesis of a Monomer M by ATRP with a Catalyst [L/Mt^x] (Mt Stands for a Generic Metal, *x* for Its Formal Oxidation State, and L/ for Its Coordination Sphere), Starting from a R_0X Initiator (X = Halogen)

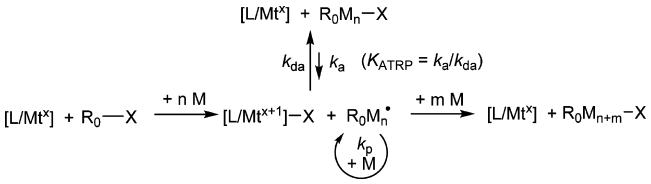

vast majority of the investigated systems are based on a reversible activation/deactivation equilibrium involving the Fe^{II}/Fe^{III} couple (i.e., $Mt^x = Fe^{II}$ in Scheme 1), supported by many different types of neutral ligands, L, including phosphines, imines, amines, and combinations thereof, with halides, alkoxides, phenolates, and others as anionic ligands.[11] One remarkable system is [$FeCl_2$(α-diimine)], where α-diimine = $R^1N{=}C(R^2)C(R^2){=}NR^1$, introduced by Gibson and co-workers and applied to the polymerization of styrene and acrylate monomers.[12−14] This system acts as a catalyst for controlled chain growth when R_2 = H, whereas complexes with R_2 = aryl lead, in general, to polymers with low-molecular weights that do not increase with conversion, indicating a catalyzed chain transfer (CCT) process.[12−14] This phenomenon was interpreted as resulting from a competing trapping of the growing radical chain by the excess Fe^{II} catalyst, leading to an organometallic Fe^{III} dormant chain that has the possibility to eliminate the chain by β-H elimination and start a new chain by insertion of monomer into the resulting Fe^{III}−H bond.[15]

This phenomenon is an example of a more general scheme, first demonstrated with Mo compounds,[16] where the three basic processes of controlled chain grown by ATRP, controlled chain growth by OMRP (organometallic mediated radical polymerization),[17−20] and CCT can interplay, because the same [L/Mt^x] species can act as ATRP catalyst, OMRP chain trap, and CCT catalyst, respectively.[21] More recently, new Fe catalysts based on a functionalized bis(phenolate) ligand have been developed that show no apparent interference of CCT.[22] The Fe^{III} complexes used to mediate the polymerizations (Scheme 2) do not have the appropriate oxidation state for

Scheme 2. Functionalized Bis(phenolate) Fe^{III} Complexes Used in the Reverse ATRP of Styrenes and MMA

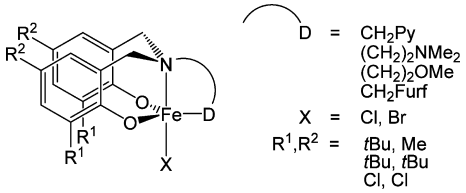

direct application as an ATRP catalyst, but they can be used under reverse ATRP conditions (R-ATRP): A conventional radical initiator is used to abstract the halogen atom, generating the ATRP Fe^{II} activator and the halide initiator *in situ*. The convenience of this method is that the Fe^{III} complex is air stable, whereas the corresponding Fe^{II} complex is extremely air sensitive. A few of these systems, particularly those with dimethylaminoethyl functionality and chlorinated phenolates, led to rapid, extremely efficient, and well controlled polymerizations of substituted styrenes and methyl methacrylates. For instance, the system with the $CH_2CH_2NMe_2$ donor, $R^1 = R^2$ = Cl and X = Br yielded a PMMA with M_n = 10500 (vs a theoretical M_n of 8378) and M_w/M_n = 1.21 at ca. 99% monomer conversion, whereas related complexes with R^1 and R^2 = alkyl gave polymers with a greater discrepancy between observed and theoretical M_n and M_w/M_n > 1.5.[22]

Two points are of interest for this system. The first point concerns the proposed mechanism of control. Experimental mechanistic investigations, carried out on the dimethylaminoethyl derivative with the 2,4-dichloro-substituted phenolates for the polymerization of styrene, suggest that the Fe complex may exert a dual (ATRP+OMRP) controlling mechanism, with the radicals being trapped by both the Fe^{III}-X and the Fe^{II} complexes to yield X-terminated and Fe^{III}-terminated dormant chains, respectively (see Scheme 3, R = Cl).[23] In this case, due

Scheme 3. Proposed Dual Controlling Mechanism for the Polymerization of Styrene

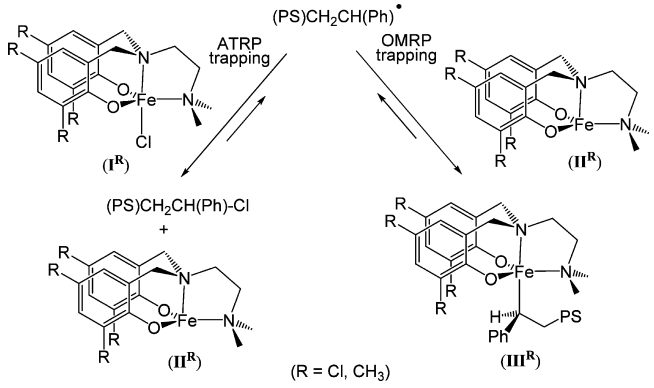

to the challenges of isolating and characterizing the parent Fe^{II} ($\mathbf{II}^{\mathbf{R}}$) and Fe^{III}-alkyl ($\mathbf{III}^{\mathbf{R}}$) species, this evidence is largely circumstantial or indirect. The second point of interest is the dramatic effect of the arene substituents R^1 and R^2 on the controlling ability of this system. Whereas the nature of the halogen X and donor function D did not significantly affect the mediator performance, only when using $R^1 = R^2$ = Cl was it possible to obtain polymers with molecular weights in agreement with theory and with narrow molecular weight distributions.

Dual (ATRP+OMRP) controlling mechanisms for radical polymerization have also been previously described for complexes of molybdenum,[16,24,25] chromium,[26] and osmium.[27] In the latter case, DFT calculations gave support for the simultaneous action of both trapping equilibria,[28] whereas for a chromium system it was concluded that control is solely imparted by OMRP trapping, even under ATRP conditions.[26] In this contribution, we present the results of a computational investigation aimed at investigating the dual controlling mechanism for the Fe complex in Scheme 3 and at understanding the peculiar effect of the arene substitution.

■ COMPUTATIONAL DETAILS

The computational work was carried out using the Gaussian09.D01 suite of programs.[29] The geometry optimizations were performed without any symmetry constraint using the BPW91, B3PW91*, B3PW91, M06, and M06L functionals. The B3PW91* is a modified version of the B3PW91 functional, in which the c3 coefficient in Becke's original three-parameter fit[30] to thermochemical data was changed to 0.15. The 6-31G basis functions were used for all atoms except Fe and Cl. The Cl atom was described with the 6-31G(d) basis

dx.doi.org/10.1021/ic5009347 | Inorg. Chem. 2014, 53, 7580−7590

set, whereas the SDD basis set and ECP were used for the Fe atom, augmented by an f polarization function (α = 2.462).[31] The unrestricted formulation was used for all open-shell molecules, yielding only minor spin contamination. Maximum deviations for $\langle S^2 \rangle$ at convergence were 0.855 (vs the theoretical value of 0.75) for spin doublets, 4.158 (vs 3.75) for quartets, 6.022 (vs 6) for quintets, and 8.767 (vs 8.75) for sextets. Corrections for dispersion on selected results were carried out at the fixed B3PW91* optimized geometries using Grimme's D3 empirical method (B3PW91*-D3), using SR6 and S8 parameters identical to those optimized for B3PW91.[32]

RESULTS

a. General Considerations. Two systems were chosen for our computational investigation, one being a system that leads to a well controlled polymerization and one for which the control is poor. Both systems contain the $Me_2NCH_2CH_2$ arm on the amine-bis(phenolate) ligand (refer to Scheme 2), the first one having $R^1 = R^2 = Cl$, the second one with $R^1 = R^2 = CH_3$. Both systems are exact replicas of catalysts studied, with the Cl derivative extensively investigated and the CH_3 system serving as a computationally inexpensive but electronically similar group to the *t*Bu functionality, as confirmed by recent experimental polymerizations.[23] Referring to the compound numbering in Scheme 3, the complexes that have been investigated will be referred to as $\mathbf{I}^{Cl}$, $\mathbf{II}^{Cl}$, $\mathbf{III}^{Cl}$ for system one and as $\mathbf{I}^{Me}$, $\mathbf{II}^{Me}$, $\mathbf{III}^{Me}$ for system two. For the organometallic dormant species **III**, the polymer chain was modeled by a 1-phenylethyl group (namely, the entire chain prior to the last monomer unit was replaced by an H atom).

Iron complexes are a particularly challenging task for computational chemistry, because of their variability of spin state that can be fine-tuned by the ligand environment.[33] Coordination compounds with low-field ligands tend to yield the highest possible spin state, namely sextet (five unpaired electrons, S = 5/2) for Fe^{III} and quintet (four unpaired electrons, S = 2) for Fe^{II}. However, alkyl ligands establish more covalent bonds with the metal center, strengthening the ligand field and leading to electron pairing phenomena in organometallic derivatives.[34] This can lead to Fe^{III} ground states with an intermediate spin (quartet, S = 3/2) or even a low spin (doublet, S = 1/2). Thus, whereas the Fe^{III}-X complex of interest in this investigation (Scheme 2) and the Fe^{II} complex that results from X atom abstraction certainly adopt a high spin state, a question arises about the possible spin state of the organometallic dormant species.

A further challenge concerns the quality of the computational method. When the interest is focused on systems that can adopt more than one possible spin state, low-level monoelectronic Hartree–Fock methods are not reliable and only more sophisticated and computationally expensive strategies that take electron correlation into account can lead to satisfactory results. On the other hand, the effects that we are probing rely on modifications in a remote area of the molecule, far from the metal. Ligand simplification is therefore not prudent. Given the size of the molecules of interest, the general method offering the best compromise in terms of accuracy and computational time is density functional theory. However, no clear guideline in terms of the best functional to use exists; benchmarking is necessary, using experimentally known systems that are as close as possible to those of interest. Previous work on Fe systems with variable spin states has shown that functionals based on the local approximation and on the generalized gradient approximation tend to overestimate the stability of the lower spin state.[35] On the other hand, hybrid functionals such as the popular B3LYP and B3PW91 show the opposite trend, generally overestimating the stability of the higher spin state.[35] The use of modified hybrid functionals, where the percent of exact Fock exchange was decreased to some extent from that of standard hybrid functionals, has often provided an optimum choice for computational accuracy.[35−39] However, no such benchmarking of this functional has been conducted for organometallic Fe^{III} systems.

b. Benchmarking Functionals on Organometallic Fe^{III} Complexes. The putative organometallic dormant species **III** (Scheme 3) could not be properly characterized in terms of its spin state properties and model compounds with simple alkyl ligands are not yet available for this system. Indeed, alkyliron(III) complexes appear as rather fragile species when supported by low-field ligands, which is indeed a reason why they are of interest in OMRP. For benchmarking purposes, we sought organometallic compounds reported in the literature that were isolable, stable and magnetically characterized.[34] Among these, we were particularly attracted by the family of (porphyrin)Fe^{III}R compounds, since the spin state was shown to depend on the nature of the alkyl group.[40] The systems were reported to adopt a high spin state (sextet) or a low spin state (doublet) depending mostly on the nature of the axial ligand (high spin for perfluoroaryl derivatives such as C_6F_5, low spin for alkyl and nonfluorinated groups). The spin state does not seem to depend on the porphyrin substituents, but we did not wish to simplify the porphyrin system for our calculations (e.g., by replacing the various substituents on the porphyrin periphery with H atoms), nor to treat these groups at the molecular mechanics level. The smallest experimentally investigated porphyrin system was tetraphenylporphyrin (TPP). Hence, we carried out calculations in the low and high spin states for (TPP)Fe(CH_3) and (TPP)Fe(C_6F_5). To reduce computational costs the spin state difference was evaluated with all functional at the fixed geometries optimized at the B3PW91* level rather than systematically reoptimizing the geometry with each functional (geometries are reported and discussed in Supporting Information (SI)). The essential energy results are shown in Table 1. However, specific reoptimizations were carried out for the high spin systems, at the BPW91 level for R = C_6F_5 and at both the BPW91 and B3PW91 levels for R = CH_3. The geometries changed insignificantly and the energy decreased only by ca. 3 kcal/mol for the BPW91 calculations and by only 0.1 kcal/mol for the B3PW91 calculation.

Table 1. Relative Energy ($E_{5/2} - E_{1/2}$ in kcal/mol) of High and Low Spin (TPP)FeR Systems (R = CH_3, C_6F_5) with Different Functionals

R	BPW91	B3PW91*	B3PW91	M06L	M06
CH_3	19.7	6.1	1.1	4.2	−16.8
C_6F_5	11.4	−0.6	−5.3	−2.7	−25.6

Since the C_6F_5 compound is known to have a high spin ground state, the results show the expected overestimation of the low spin state stability for the BPW91 functional. Conversely the M06 functional, which performs satisfactorily when applied to problems of long-range weak interactions, incorrectly predicts a high spin ground state for the CH_3 derivative. Thus, these two functionals are unsuitable for transition metal spin state predictions. The B3PW91, B3PW91* and M06L functionals correctly predict the ground

dx.doi.org/10.1021/ic5009347 | Inorg. Chem. 2014, 53, 7580−7590

Table 2. Selected Parameters for Compounds I^{Me} and I^{Cl}

	I^{Me}			I^{Cl}	
parameters[a]	X-ray[b]	DFT (sextet)	DFT (quartet)	DFT (sextet)	DFT (quartet)
Fe−Cl	2.29(1)	2.284	2.262	2.254	2.225
Fe−NMe_2	2.152(2)	2.226	2.214	2.211	2.200
Fe−N	2.288(2)	2.363	2.138	2.377	2.118
Fe−O	1.855(2), 1.868(2)	1.857, 1.862	1.837, 1.851	1.866, 1.872	1.853, 1.864
Cl−Fe−N	170.1(1)	170.1	177.3	171.2	178.5
Cl−Fe−NMe_2	92.2(1)	91.6	98.7	92.6	96.9
Cl−Fe−O	94.3(1), 99.4(1)	99.9, 100.0	90.4, 91.7	100.0, 100.7	91.0, 91.6
N−Fe−NMe_2	79.7(1)	78.5	83.9	78.7	84.2
O−Fe−N	85.6(1), 89.1(1)	84.4, 84.1	88.5, 88.6	83.1, 83.5	87.8, 89.2
O−Fe−O	121.3(1)	127.5	163.2	128.1	159.8
τ	0.813	0.710	0.235	0.718	0.312
q(Fe)		0.669	0.488	0.701	0.516
q(Cl)		−0.329	−0.287	−0.277	−0.214
ΔE		**0.0**	**13.8**	**0.0**	**15.5**

[a]Distances in angstroms, angles in degrees, effective charges in electrons, ΔE in kcal/mol. [b]From ref 41.

state for both compounds. Unfortunately no quantitative indications of the doublet-sextet gap are available for these compounds from the experimental studies. On the basis of the established suitability of B3PW91* to other Fe chemistry,[35−39] we have elected to continue our investigations with this modified hybrid functional.

c. The ATRP Equilibrium. For system **I**, an X-ray structure is available in the literature for $\mathbf{I}^{Me}$,[41] providing the opportunity to test the suitability of the functional to reproduce experimental geometries. The complex was also shown to adopt a high spin ground state from magnetic susceptibility measurements. However, we have also carried out the geometry optimization of the quartet ground state, for later comparison with the quartet alkyl species **III**. The selected bond distances and angles reported in Table 2 demonstrate good agreement between the experimental and optimized geometry. The greatest discrepancy concerns the bond distances to the neutral N donor atoms, Fe−NMe_2 (eq) and Fe−N (ax), which are overestimated by ca. 0.08 Å. Representations of the optimized structures are shown in Figure 1. On going from the sextet to the quartet state for each compound, structural changes are largely as expected: a general shortening of the bond lengths is observed, in particular the Fe−N (ax) bond (ca. 0.2 Å), with a concomitant widening of the O−Fe−O angle. Thus, while the sextet structure is closer to an ideal trigonal bipyramid, the quartet structure can better be described as a distorted square pyramid, with the NMe_2 donor group occupying the apical position. This geometrical change can be conveniently monitored by the well-known τ parameter,[42] the values of which for the different structures are also reported in Table 2. The large bond shortening is accentuated by the fact that the high spin configuration contains one electron in a metal−ligand antibonding orbital, which is removed upon electron pairing when switching to the intermediate spin configuration. On going from $\mathbf{I}^{Me}$ to $\mathbf{I}^{Cl}$, there is a slight shortening of the Fe^{III}−Cl distance (by 0.03 Å in the sextet state and 0.04 Å in the quartet state). This may be attributed to an increase of the effective positive charge on the Fe atom, as a result of the inductive effect of the phenolate ring Cl substituents. Indeed, the calculated Mulliken charge on Fe increases on going from $\mathbf{I}^{Me}$ to $\mathbf{I}^{Cl}$ (Δq(Fe) = +0.032). This inductive effect causes a greater transfer of charge from the Cl ligand to Fe, a greater covalence, and a stronger bond, correlating with the decreased negative charge of the Cl^- ligand (Δq(Cl) = +0.052). Note that this effective charge is reduced more significantly when moving from the sextet to the quartet state and the Fe positive charge is consequently reduced. This is associated with the removal of one electron from an antibonding orbital and with the Fe−Cl bond shortening and agrees with the expected greater Fe−Cl bond covalence in the lower spin state. The calculations yield greater stability for the sextet state, in agreement with the experimental evidence, with a sextet−quartet gap that is only slightly greater for $\mathbf{I}^{Cl}$. The optimizations of the $\mathbf{I}^{Me}$ sextet and quartet systems were also carried out at the M06 level, yielding a much greater sextet−quartet gap and a less accurate geometry

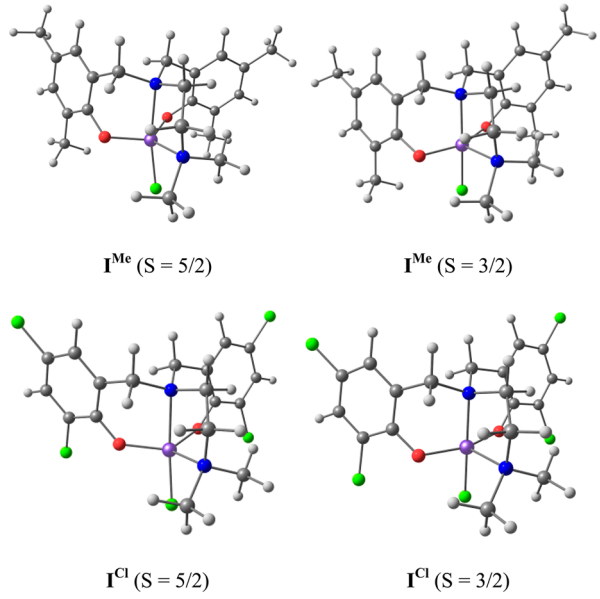

Figure 1. Views of the optimized geometries of $\mathbf{I}^{Me}$ and $\mathbf{I}^{Cl}$ in the sextet and quartet states.

dx.doi.org/10.1021/ic5009347 | Inorg. Chem. 2014, 53, 7580−7590

for the sextet (further details are provided in the SI). This confirms that M06 is a less suitable functional for this system.

System **II** has not been structurally characterized. This extremely air sensitive compound could be isolated in the case of $\mathbf{II}^{Cl}$, but only with cocrystallized LiCl to yield a $Fe_2Li_2Cl_2$-core dinuclear species.[23] A possible reason for the instability of this complex is the tension imposed by the tetradentate ligand, not allowing relaxation to the preferred tetrahedral geometry for 4-coordinate Fe^{II}. The geometry optimization of **II** was carried out only in the quintet state, the undoubtedly preferred spin state for this complex given the low coordination number and the weak ligand field, as experimentally verified for other similar compounds (i.e., $FeCl_2(\alpha$-diimine$)$).[43] The selected bonding parameters are collected in Table 3, and optimized

Table 3. Selected Parameters for Compounds $\mathbf{II}^{Me}$ and $\mathbf{II}^{Cl}$

parameters[a]	$\mathbf{II}^{Me}$	$\mathbf{II}^{Cl}$
Fe−NMe_2	2.193	2.174
Fe−N	2.166	2.170
Fe−O	1.891, 1.903	1.895, 1.908
N−Fe−NMe_2	84.4	85.0
O−Fe−N	95.7, 95.5	94.7, 94.3
O−Fe−O	144.5	144.5
q(Fe)	0.610	0.675

[a]Distances in angstroms, angles in degrees, effective charges in electrons.

geometries are shown in Figure 2. The effective charge increase for the Fe atom on going from $\mathbf{II}^{Me}$ to $\mathbf{II}^{Cl}$ (Δq = +0.065) is greater than that for system **I** (Δq = +0.032).

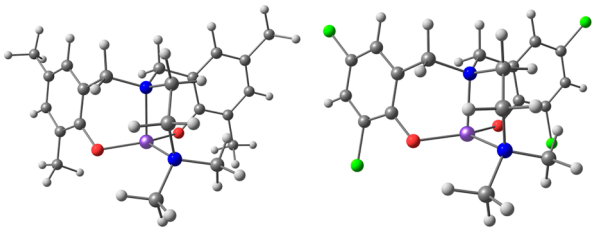

Figure 2. Views of the optimized geometries of spin quintet $\mathbf{II}^{Me}$ (left) and $\mathbf{II}^{Cl}$ (right).

Geometry optimization and energy calculation for the $PhCH(Cl)CH_3$ molecule and $PhCHCH_3$ radical as models of the ATRP dormant and grown radical chain, respectively, allow estimation of the ATRP equilibrium (eq 1). The energy

$$\mathbf{II} + PhCH(Cl)CH_3 \underset{k_{da}}{\overset{k_a}{\rightleftharpoons}} \mathbf{I} + PhCHCH_3^{\bullet} \quad (1)$$

difference calculated for this equilibrium is +3.6 kcal/mol for $\mathbf{II}^{Me}/\mathbf{I}^{Me}$ and +8.6 kcal/mol for $\mathbf{II}^{Cl}/\mathbf{I}^{Cl}$. After applying a dispersion correction to these data (B3PW91*-D3, see Computational Details), these values changed only slightly to 2.1 and 7.2 kcal/mol, respectively.

d. OMRP Equilibrium. The OMRP equilibrium involves species **II** (*vide supra*) as a spin trap and **III** as dormant species (eq 2). The latter was modeled by shortening the polymer chain to the $CH(Ph)CH_3$ group.

The geometry optimization of **III** was the most challenging part of this study, because stable model compounds do not exist

$$\mathbf{III} \underset{k_{da}}{\overset{k_a}{\rightleftharpoons}} \mathbf{II} + PhCHCH_3^{\bullet} \quad (2)$$

and the spin state is unknown. Given the large size of the molecule, a preliminary investigation was carried out on a system containing a simple CH_3 as the alkyl group and H atoms on the 2 and 4 positions of the phenolate benzene rings. This system, abbreviated as $\mathbf{III}^{H}$, was optimized in all possible spin states (sextet, quartet, and doublet). The details of the optimized structures are given in the SI. The energetic results are in favor of an intermediate spin state for this system, slightly more stable than the high spin state (at +4.6 kcal/mol relative to the quartet) and much more stable than the low spin state (at +18.9 kcal/mol). Calculations on a related system, a $Fe(CH_2Ph)Cl_2(\alpha$-diimine$)$ complex, also yielded a quartet state lower than the sextet, whereas the doublet state was not calculated.[44] Using the fixed B3PW91* geometries for single point calculations and restricting the analysis to the quartet−sextet gap, the other functionals also yielded a quartet ground state ($E_{sext} - E_{quart}$ = 8.5 for BPW91, 3.1 for B3PW91, and 0.9 kcal/mol for M06L) except for the M06 functional, for which the sextet state was found to be more stable than the quartet by 3.2 kcal/mol. The subsequent calculations on the full system were therefore carried out only in the quartet state.

It is interesting to observe that, upon increasing the ligand field strength from halide to alkyl, the preferred high spin state of the former switches to the low spin state for the alkylporphyrin systems (*vide supra*) while the intermediate spin state is favored for the diaminobis(phenolato)alkyl system. This is certainly related to the different constrained geometries of the two systems: the porphyrin derivatives force the strong alkyl ligand to occupy the apical position of a square pyramidal geometry, therefore inducing strong destabilization of the $d_{x^2-y^2}$ orbital and d_{z^2} orbitals, whereas system **III** can accommodate the alkyl group in a pseudobasal position.

Indeed, the geometry of **III**, shown in Figure 3, is closer to a square pyramid than to a trigonal bipyramid, with quite similar

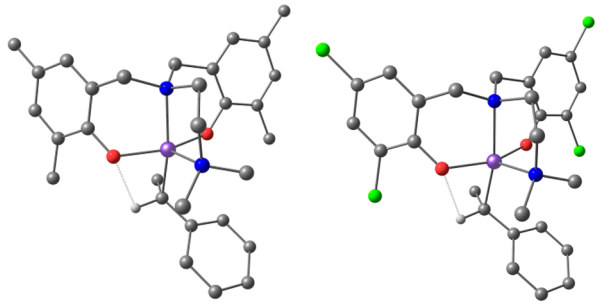

Figure 3. Views of the optimized geometries of spin quartet $\mathbf{III}^{Me}$ (left) and $\mathbf{III}^{Cl}$ (right). For clarity purposes, the H atoms are not shown except for the α-H of the alkyl ligand (additional representations available in the SI).

angular parameters to those of the quartet chloride analogue (cf. Table 4 with Table 2) and with the 1-phenylethyl group occupying a pseudobasal position. However, all the bonds between the Fe atom and the diaminobis(phenolate) ligand are significantly longer in **III** relative to **I** with the same ligand. The Fe−NMe_2 and Fe−O distances in **III** are even longer than those in the corresponding complex **I** in the higher (sextet) spin state, whereas the Fe−N distances in **III** are shorter than the same distances in sextet **I**, but still >0.1 Å longer than those

dx.doi.org/10.1021/ic5009347 | Inorg. Chem. 2014, 53, 7580−7590

Table 4. Selected Parameters for Compounds III^{Me} and III^{Cl}

parameter[a]	III^{Me}	III^{Cl}
Fe−C	2.162	2.202
Fe−NMe_2	2.255	2.224
Fe−N	2.229	2.248
Fe−O	1.903, 1.907	1.923, 1.918
C−Fe−N	168.3	167.0
C−Fe−NMe_2	110.1	110.9
C−Fe−O	86.5, 90.5	86.1, 91.4
N−Fe−NMe_2	81.5	81.9
O−Fe−N	88.9, 89.2	88.0, 88.5
O−Fe−NMe_2	101.0, 102.8	101.4, 104.8
O−Fe−O	155.5	152.9
τ	0.213	0.235
O···α-H	2.302	2.320
Fe−C−H	93.8	92.8
q(Fe)	0.613	0.644

[a]Distances in angstroms, angles in degrees, effective charges in electrons.

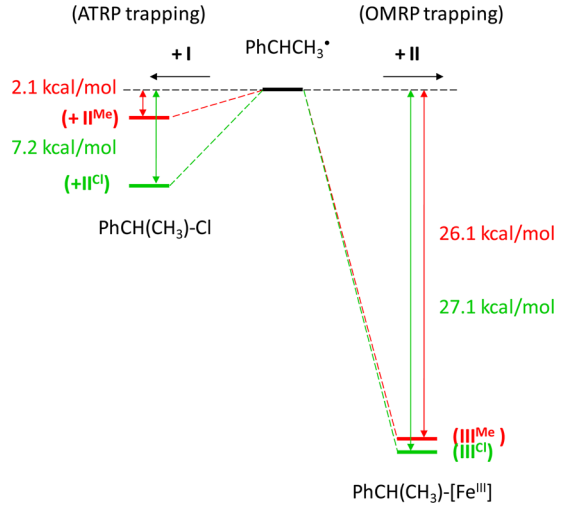

Figure 4. Energy diagram summarizing the ATRP and OMRP activation/deactivation equilibria from the B3PW91*-D3 calculation for systems $I^{Me}/II^{Me}/III^{Me}$ and $I^{Cl}/II^{Cl}/III^{Cl}$.

in quartet **I**. This peculiar effect may be related to the greater steric encumbrance of the alkyl group in **III** relative to Cl in **I**. The most stable optimized geometry has the methyl group of the 1-phenyethyl ligand facing the "empty" coordination site, underneath the square base, opposite to the apical NMe_2 ligand. An alternative rotamer where the phenyl group faces the same site (shown in SI) is slightly higher in energy (+4.6 kcal/mol). A possible reason for this energy difference is a weak interaction between the α-H atom and one of the phenolate O atoms. This is also supported by the small Fe−C−H angle, approaching 90° (Table 4). In the higher energy isomer, the steric preference of the Ph ring forces the α-H atom to be further away from the O atom (2.539 Å) with an expanded Fe−C−H angle of 97.8°.

The effect of the 2,4-dichloro substitution on the phenolate benzene rings is opposite relative to **I** and **II**: on going from III^{Me} to III^{Cl}, the distance to the alkyl ligand significantly lengthens. The effective positive charge on the Fe atom increases, as expected on going from III^{Me} to III^{Cl}, but this time it does not result in a bond strengthening, perhaps because the Fe−C bond has a greater covalent nature relative to the Fe−Cl bond. Taking into account the energy of the $PhCHCH_3^{\bullet}$ radical, the energy change for the OMRP equilibrium of eq 2 is calculated as 8.0 kcal/mol for the II^{Me}/III^{Me} system and 9.4 kcal/mol for the II^{Cl}/III^{Cl} system. These calculations were more strongly affected by the dispersion correction than those of the ATRP equilibrium. The B3PW91*-D3 calculations yielded 26.1 and 27.1 kcal/mol, respectively. The large increase of BDE by ca. 18 kcal/mol on going from B3PW91* to B3PW91*-D3 is comparable to that reported recently for the BDE of methylcobalamin on going from B3LYP to B3LYP-D (ca. 15 kcal/mol).[45] The underestimation of BDE's by hybrid functionals and the effect of the dispersion correction on these calculations is well established.[46,47] The reason for the small effect of the dispersion correction on the ATRP equilibrium is the cancellation of error given the compensation of one bond breaking with one bond making.

e. Comparison of the Two Equilibria and Dual Control. The energetic results of the ATRP and OMRP activation/deactivation equilibria for the two investigated systems are summarized in Figure 4. They indicate that the system with the 2,4-dichloro-substituted phenolate ligands affords more stable dormant species for both ATRP and OMRP deactivation modes. The relative stabilization trends can be understood on the basis of the electron withdrawing effect of the 2,4-Cl substituents on the phenolato benzene rings. These electron-withdrawing Cl atoms disfavor the ATRP activation because they remove electron density from Fe^{II}, making it more difficult for the system to be further oxidized to Fe^{III}−Cl by the ATRP activation process. The calculated Mulliken charges support this view, with the charge of +0.610 in II^{Me} becoming +0.669 in I^{Me} (Δq = +0.059) for the dimethyl-substituted system, whereas the same process for the dichloro system involves a metal charge increase from +0.675 in II^{Cl} to +0.701 in I^{Cl} (Δq = +0.026). In the formation of the organometallic dormant species, on the other hand, the newly formed Fe^{III}−$CH(Ph)CH_3$ bond is less polar, given the lower electronegativity of carbon. The metal charge changes very little during the OMRP trapping process for the dimethyl system (from +0.610 in II^{Me} to +0.613 in III^{Me}; Δq = +0.003) and actually decreases for the dichloro system from +0.675 in II^{Cl} to +0.644 in III^{Cl} (Δq = −0.031). We can therefore assume that the Fe−C bond formation in the OMRP trapping process provides better stabilization for the dichloro derivative.

Good control in RDRP occurs when the active radical species equilibrates with at least one thermodynamically favored dormant species. Greater relative stability of the dormant species leads to better control by promoting lower radical concentrations. Thus, the results in Figure 4 agree with the experimental evidence of better control imparted by the $I^{Cl}/II^{Cl}/III^{Cl}$ system. More specifically, the polymerization is well controlled when carried out under ATRP conditions, although a significant fraction of the polymer chain-ends were not halogen end-capped. The dynamics of the controlled polymerization process in the presence of an ATRP/OMRP interplay is well understood[21] and will briefly be summarized here: activation under ATRP conditions (from either L/Mt^x and R_0−X, see Scheme 1, or from L/Mt^{x+1}−X and $R_0^{\bullet}$ as in the present case) generates the propagating radicals in equilibrium with the halogen-terminated dormant chain plus the catalyst **II**. However, since the ATRP equilibrium is displaced toward complex **II**, this complex is also available to trap the active chains, leading to the OMRP dormant chain **III**. The OMRP

dx.doi.org/10.1021/ic5009347 | Inorg. Chem. 2014, 53, 7580−7590

trapping synergistically interplays with the ATRP trapping to further decrease the steady-state radical concentration in solution and to increase the system controllability. When initiated under ATRP conditions, concurrent OMRP trapping cannot be avoided. However, when initiated under OMRP conditions, the polymerization can be regulated by just this mechanism, without participation of ATRP trapping. A styrene polymerization experiment carried out under OMRP initiation conditions with system $\mathbf{II}^{Cl}$, which was generated by *in situ* reduction of $\mathbf{I}^{Cl}$ with ascorbic acid, and AIBN as radical source gave again a controlled polymerization, although not as well controlled as in the presence of the two synergistically interplaying equilibria.[23] However, as the *in situ* reduction by ascorbic acid is likely not complete in the time scale of the initiation to establish the dynamic equilibria, it is difficult to eliminate a mixed, or indeed an ATRP-only, mechanism from operating.

f. Interpretation of Computational Results When Predicting Experiment. Several notes of caution should be made regarding the veracity of conclusions drawn. The first is the suggestion from the computational data that the OMRP equilibrium would be the dominant control mechanism in this system. It is dangerous to draw quantitative significance from the calculated energy differences. As pointed out at the beginning of the Results section, the choice of functional highly affects the absolute energy values and also the relative ones since there is a change of spin state during the activation/deactivation process. Although benchmarking has guided us toward the B3PW91* functional, which gives qualitatively correct results for the ground state of known alkyl-Fe^{III} complexes, the absolute ΔE values obtained for the present system should not be considered as reliable, especially since they also heavily depend on the correction applied for dispersion effects. What are more reliable are the observed trends within each equilibrium (ΔE_{ATRP} and ΔE_{OMRP}), where errors effectively cancel, on going from the dimethyl to the dichloro system. Even comparing the absolute ΔE_{ATRP} and ΔE_{OMRP} values for the same system as an indication of trapping efficiency is not quantitatively reliable: Equilibria depend on ΔG, not ΔE. Whereas the ATRP trapping process involves one metal complex and one small organic molecule on each side, hence $\Delta G \sim \Delta E$ (the $T\Delta S$ term is small), the OMRP trapping process leads to disappearance of one small molecule ($\Delta S < 0$); thus, the ΔG stabilization is smaller than the computed ΔE. Calculating these ΔG values by DFT with the standard gas phase approximation would not provide reliable numbers, as these reactions occur in a condensed phase, where translational and rotational modes are significantly quenched. Even calculating the thermochemical parameters in solution by a polarizable continuum method does not provide an ideal solution, as pointed out in various theoretical contributions.[48−51] Therefore, we purposely avoided making additional corrections of uncertain value (except for the recommended correction for dispersion[52]) and prefer to directly present the original gas phase electronic energy data. From a strictly qualitative point of view, the ATRP equilibrium stabilization is probably not significantly affected by thermal, entropy, and solvent corrections, especially in nonpolar media such as the styrene monomer itself, used in the bulk polymerization experiments. The OMRP equilibrium stabilization, on the other hand, is likely to be less important on the G scale than the calculated ΔE value. This consideration is also in agreement with the experimental observations. First, styrene polymerization mediated by $\mathbf{I}^{Cl}$ is controlled more poorly by an ascorbic acid reduction facilitating an OMRP-initiation than by ATRP +OMRP. If the relative stabilization of the dormant species was as indicated in Figure 4 on a Gibbs energy scale, OMRP should provide the major controlling mechanism and perhaps lead to good control even in the absence of ATRP. Second, styrene was less efficiently controlled by $\mathbf{I}^{Me}$ under the ATRP+OMRP regime than by $\mathbf{I}^{Cl}$ under the OMRP only regime, supporting our doubt of quantitative relevance. Finally, it is important to note that this is an idealized system. In an experimental operation, protic impurities would surely react vigorously with the organometallic trapping intermediates, decomposing catalysts and minimizing observed OMRP trapping. Thus, this computational work suggests that the OMRP trapping mechanism is accessible and helps to improve the control alongside a dominant ATRP controlling mechanism. The same proverbial grain of salt should be taken with the analysis, to follow in the subsequent sections, of the effect of electronic structure on trapping barriers and the role pressure plays in controlling these equilibria.

g. Effect of the Electronic Structure on the Trapping Barriers. Considering the spin state variability for Fe^{II} and Fe^{III} complexes and the ground state dependence on the coordination geometry, it is of interest to examine the effect of the spin state on the reaction coordinate. Reactions with a change of spin state between reagents and products, termed two-state reactions[53] or spin crossover reactions,[34,54] may be characterized by greater activation barriers relative to analogous single state reactions for enthalpic and/or entropic reasons, the former related to the possible need to reach a crossover point between the two potential energy surfaces, and the latter related to a "forbiddenness" factor.[55,56] For the OMRP trapping process, while the trapping species is most definitely a spin quintet ($S = 2$) Fe^{II} complex, the resulting R−Fe^{III} dormant species has a quartet ($S = 3/2$) ground state for this particular system, but the sextet state ($S = 5/2$) is also close in energy and may become the ground state for other systems. The spin doublet ($S = 1/2$) state is much higher in energy for this system, but it could also become the ground state for other coordination geometries and ligand sets (e.g., see section b). The combination of trapping Fe^{II} complex and organic radical ($S = 1/2$) yields two degenerate states with $S = 2 \pm 1/2$ (5/2, 3/2) depending on whether the radical spin is parallel or antiparallel to the metal spin. Hence, a pathway without spin crossover can be envisaged for the trapping processes, leading to both the sextet and the quartet R−Fe^{III} species, whereas there should be at least one spin crossover point for the reaction coordinate leading to a spin doublet R−Fe^{III} species.

We have explored the reaction coordinate for the OMRP trapping leading to both the quartet and the sextet state alkyl product, limited however to the better performing $\mathbf{II}^{Cl}/\mathbf{III}^{Cl}$ system, by performing partial optimizations at various fixed Fe−C distances. The association process (from right to left in Figure 5) proceeds smoothly, without any apparent barrier, for both spin states. The profile for the quartet state is that of a typical Morse-type dissociation curve. Interestingly, for a Fe−C distance as short as 3.9 Å, the energy of the sextet is still essentially degenerate with the quartet state, even though the system is already energetically stabilized by ca. 3 kcal/mol relative to the dissociation asymptote. Thus, the orbital interaction is already sufficiently developed to provide a significant energetic stabilization that is independent of the relative orientation of the two spins. At shorter distances,

dx.doi.org/10.1021/ic5009347 | Inorg. Chem. 2014, 53, 7580−7590

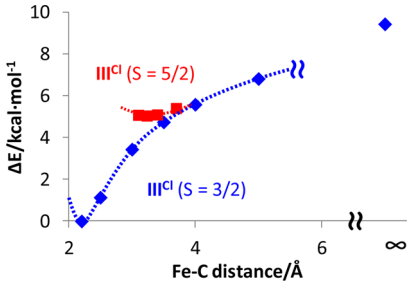

Figure 5. Reaction coordinates for the OMRP equilibrium process through partial optimizations of $\mathbf{III}^{Cl}$ at various fixed Fe−C distances.

however, while the quartet drops significantly in energy, the sextet remains essentially at the same energy, converging to a stable minimum with a long Fe−C distance of 3.236 Å and an energy 5.0 kcal/mol higher than that of the quartet. The geometry of the optimized sextet is given in the SI. Hence, this analysis suggests that OMRP trapping should be a fast process whenever a spin quintet Fe^{II} complex leads to a dormant species in either a quartet or a sextet ground state.

A qualitative orbital diagram of the Fe−C bond formation process may be conceived as shown in Scheme 4. For the formation of the quartet product, resulting from an antiparallel combination of the reagent spins, two antiparallel electronic spins can couple directly to form the $R-Fe^{III}$ bond (right-hand side in Scheme 4), consistent with the absence of an electronic barrier. The interaction leading to the sextet ground state, on the other hand, involves a parallel orientation of the reagent spins. The formation of the Fe−C bond involves an electronic reorganization with involvement of the "down" electron from a Fe^{II} nonbonding metal orbital, whereas the "up" electron occupying the metal orbital used for the bond ends up in the $R-Fe^{III}$ antibonding combination. This view is obviously rather idealized. Evidently, the effects of the stabilizing orbital interaction and of the destabilizing antibonding electron manifest themselves at different points along the reaction coordinate.

Scheme 4. Qualitative Orbital Interaction Diagram and Reaction Coordinate for the $R-Fe^{III}$ Bond Formation (OMRP Trapping Process) from the Spin Quintet Fe^{II} Trapping Species for the Two Cases of a Quartet Ground State (right) and a Sextet Ground State (left)

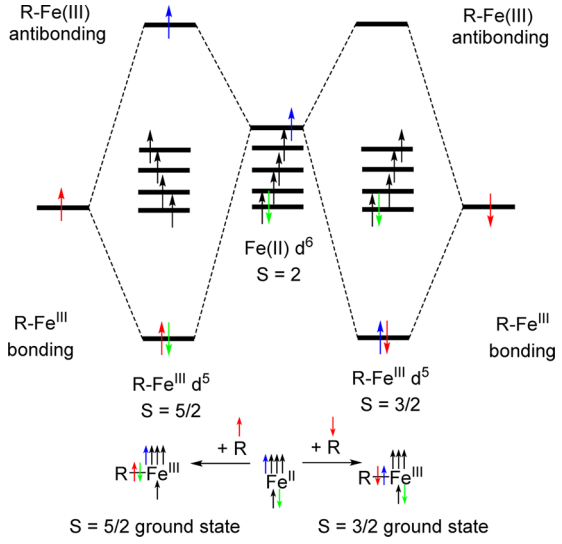

Concerning the ATRP trapping process, the $Cl-Fe^{III}$ trapping species is characterized by a high spin state (sextet, $S = 5/2$). This is likely the case for all Fe^{II}-based ATRP catalysts reported so far. The combination of $Cl-Fe^{III}$ and the radical yields two degenerate states with spin $5/2 \pm 1/2$ (3, 2), of which the second one correlates with the spin state of the Fe^{II} product. Therefore, the ATRP trapping process is also a single state reaction. As shown in Scheme 5, this reaction coordinate is also expected to involve an electronic redistribution because the new metal-based orbital generated in the Fe^{II} complex from the $Cl-Fe^{III}$ bond/antibond combination contains one unpaired electron formally deriving from the $Cl-Fe^{III}$ antibond; thus, one of the two electrons originating from the $Cl-Fe^{III}$ bond (shown in green in Scheme 5) must shift to another metal-based orbital to generate a metal based lone pair, whereas the other $Cl-Fe^{III}$ bonding electron couples with the radical electron to generate the R−Cl bond.

Scheme 5. Qualitative Orbital Interaction Diagram and Reaction Coordinate for the ATRP Trapping Process Involving Cl Atom Transfer from the Spin Sextet $Cl-Fe^{III}$ Complex to the Organic Radical R, with Formation of a Spin Quintet Fe^{II} Complex

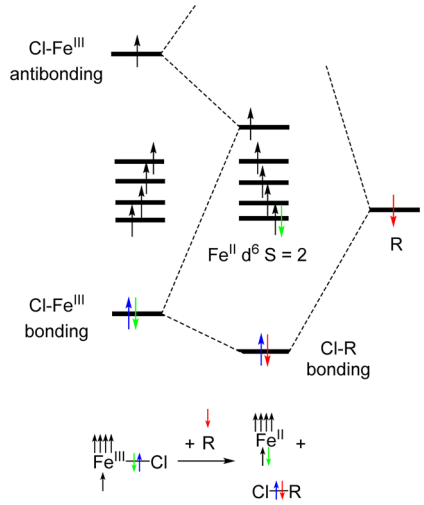

The reaction coordinate was explored by carrying out partial optimizations at intermediate positions along the reaction coordinate (Cl atom transfer), as measured in this case by the Fe−Cl distance. The results are shown in Figure 6. A first point

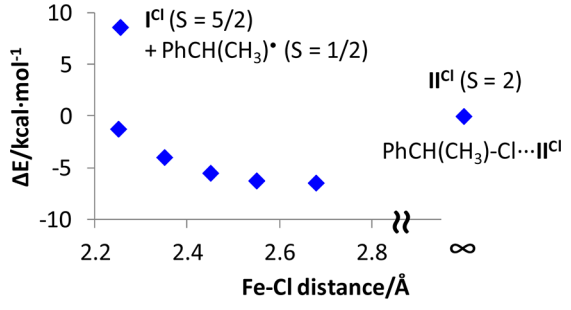

Figure 6. Reaction coordinates for the ATRP equilibrium process through partial optimizations of $PhCH(CH_3)\cdots Cl\cdots \mathbf{II}^{Cl}$ at various fixed Fe−Cl distances.

dx.doi.org/10.1021/ic5009347 | Inorg. Chem. 2014, 53, 7580−7590

of interest is the presence of a local minimum for a Lewis acid−base adduct between the ATRP catalyst $\mathbf{II}^{Cl}$ and $PhCH(CH_3)$-Cl, energetically stabilized by 6.4 kcal/mol relative to the sum of the two separate molecules. The Fe···Cl distance (2.679 Å) is already rather short and indicative of a significant donor−acceptor interaction, even though the S = 2 state of the Fe^{II} complex can only offer half-filled valence shell orbitals (see Scheme 5) to establish new bonds. Hence, the Cl → Fe donor−acceptor interaction must push one metal electron up in energy in an antibonding molecular orbital. For comparison, the Fe−Cl distance in the $\mathbf{I}^{Cl}$ product, where there is also one antibonding electron, is shorter at 2.254 Å (Table 2), which is related to its covalent rather than dative nature. R−X → Mt interactions have previously been calculated for other models of ATRP catalyst/initiator combinations. In the case of the $CH_3CH(Cl)COOCH_3$−$RuCl_2(PH_3)_2$ combination model for the initiating system of Sawamoto's $RuCl_2(PPh_3)_3$ catalyst,[57] a stabilization of 5.8 kcal/mol was calculated with a slightly different level of theory (B3LYP functional) for the interaction that involves an empty metal orbital,[58] whereas other molecules that can only provide singly occupied metal orbitals ($CpMoCl_2(PH_3)_2$ or $MoCl_3(PH_3)_3$, models of other efficient catalysts[16,59]) were found to yield repulsive interactions.[58] The positive interaction in the present case may be attributed to the greater tolerance of the harder, first row transition metal to the presence of antibonding electrons and to the lower steric encumbrance relative to the second row systems investigated in the previous study. This contrasts the computational analysis of $CH_3CH(Cl)OOCCH_3$−CpCr(ArN═CH−CH═NAr), where Ar = $C_6H_3R_2$-2,6 and R = H, Me, *i*Pr;[26] this system can also only offer half-filled metal orbitals to establish new bonds, but the steric encumbrance is greater and the interaction was found to be repulsive.

A second point of interest is the smooth energy change as the Fe−Cl distance shortens toward the value of the distance (2.254 Å) in optimized $\mathbf{I}^{Cl}$. For a frozen distance of 2.25 Å, the energy value is still *lower* than that of the separate products, $\mathbf{I}^{Cl}$ and $PhCH(CH_3)^{\bullet}$ radical, by 9.8 kcal/mol. Full optimization with release of the Fe−C distance constraint starting from this partially optimized structure relaxed the geometry back to the $PhCh(CH_3)Cl\cdots\mathbf{II}^{Cl}$ adduct. These results suggest the presence of a significant interaction between the radical and the Cl atom of compound $\mathbf{I}^{Cl}$, making the atom transfer process not only energetically favorable but also barrierless. This positive interaction may be associated with the significant spin density on the Cl atom (0.229 according to the Mulliken analysis, vs 4.060 on the Fe center), due to the electron being located in the antibonding orbital with significant Fe−Cl character (see Scheme 5). Hence, the positive interaction between this electron and the antiparallel spin on the alkyl radical is an efficient entry into the atom transfer pathway. This situation differs substantially from the atom transfer pathway calculated for the aforementioned $CH_3CH(Cl)OOCCH_3$−CpCr(ArN═CH−CH═NAr) system, where the interaction between the S = 3/2 Cl−Cr^{III} moiety and the alkyl radical is repulsive, leading to a significant barrier to the atom transfer process. In this case, the spin density for the Cr^{III} complex is nearly fully localized on the metal atom (the unpaired electrons are on pure metal based *d* orbitals: for the $C_6H_3R_2$-2,6 derivatives with R = H, Me, and *i*PrPh, the calculated spin densities are respectively 3.072, 3.071, and 3.086 on the Cr atom and 0.022, 0.017, and 0.019 on the Cl atom) and the interaction occurs with parallel spins, leading through a single-state pathway from the S = 3/2 + 1/2 combination to the S = 2 ground state of the Cr^{II} ATRP catalyst.

In conclusion, ATRP processes with Fe^{II} catalysts are likely to be associated with single-state pathways with either a relatively low activation barrier or no barrier at all, because Fe^{II} and X−Fe^{III} (X = Cl, Br) species are always likely to adopt a high spin configuration (quintet and sextet, respectively), providing evidence for the efficacy of iron in these controlled radical polymerizations. The OMRP trapping process, however, is likely to be most efficient (low or zero activation barrier) when leading to a R−Fe^{III} dormant species with either a quartet or a sextet ground state, as in the diamine-bis(phenolato) system under specific scrutiny in this contribution.

h. Effect of Pressure. A final point for consideration in this contribution is the effect of pressure on the rate of styrene polymerization mediated by systems **I**. Under the steady-state approximation for the radical concentration, the rate law for a polymerization process that takes place in the ATRP or OMRP regime is as shown in eqs 3 and 4, respectively, where K_{ATRP} and K_{OMRP} are the thermodynamic equilibrium constants for the corresponding activation/deactivation equilibria ($K = k_a/k_{da}$) of eqs 1 and 2, and k_p is the propagation rate constant. The pressure dependence of a reaction rate is reflected by the activation volume, which corresponds to the sum of the reaction volume for the activation/deactivation pre-equilibrium of interest (V_{ATRP} or V_{OMRP}) and the activation volume of the free radical propagation step ($V^{\ddagger}_{p}$).

$$v = K_{ATRP}k_p\frac{[Fe^{II}][R-Cl]}{[Cl-Fe^{III}]}[M] \qquad V^{\ddagger} = V_{ATRP} + V^{\ddagger}_{p} \tag{3}$$

$$v = K_{OMRP}k_p\frac{[R-Fe^{III}]}{[Fe^{II}]}[M] \qquad V^{\ddagger} = V_{OMRP} + V^{\ddagger}_{p} \tag{4}$$

The effect of pressure was shown to be positive both on the free radical propagation step (negative $V^{\ddagger}_{p}$) and on the activation/deactivation equilibrium for the Cu-catalyzed ATRP of styrene (negative V_{ATRP}).[60,61] The ATRP equilibrium for the $FeBr_2/FeBr_3$ couple in polar solvents S (*N*-methylpyrrolidin-2-one and acetonitrile), however, was shown to be disfavored by pressure (positive V_{ATRP}), supposedly because of the pressure-induced formation of $[Fe(S)_6]^{2+}$ species.[62] Preliminary high-pressure studies of the styrene polymerization mediated by $\mathbf{I}^{Cl}$ have demonstrated faster polymerizations at high pressures and raise their own questions about the mechanism of action in these systems, in apparent contradiction with the ATRP +OMRP model.[63] In order to learn more about this phenomenon and to see whether either the ATRP mechanism or the OMRP mechanism or both could have a positive influence of pressure on the polymerization rate, we have carried out volume calculations on the optimized structures of the species involved in the two equilibria. The results are reported in Table 5. For the ATRP activation process, there is an expected volume increase on going from **II** to **I** (40.7 cm^3/mol for the CH_3 system, 30.8 cm^3/mol for the Cl system), which is greater than the volume decrease associated with the transformation of the dormant species to the active radical (−11.5 cm^3/mol). Consequently, V_{ATRP} is positive and is predicted to have a negative effect on the polymerization rate at high pressure. Conversely, the molar volume decrease associated with the transformation of **III** to **II** (−158.0 cm^3/mol for the CH_3 system, −109.3 cm^3/mol for the Cl system) is

dx.doi.org/10.1021/ic5009347 | *Inorg. Chem.* 2014, 53, 7580−7590

Table 5. Calculated Molecular Volumes (cm^3/mol) for the Species Involved in the ATRP and OMRP Equilibria

	dimethyl system	dichloride system
PhMeCH•	89.5	
PhMeCH−Cl	101.0	
I (S = 5/2)	298.0	310.6
II (S = 2)	257.3	279.8
III (S = 3/2)	415.3	389.1
ΔV_{ATRP}	29.2	19.3
ΔV_{OMRP}	−68.5	−19.8

greater than the volume loss associated with the generation of the free radical (89.5 cm^3/mol). This trend can be attributed to the shortening of all the bonds between the Fe atom and the donor atoms of the diaminobis(phenolato) ligand (cf. Tables 3 and 4). Consequently, and perhaps counterintuitively, V_{OMRP} is negative and is predicted to have a positive effect on the polymerization rate at high pressures.

It is important to point out that the calculated molar volume changes for the two controlling equilibria do not take into account solvation effects. Solvation may have a dramatic effect on the volume change in RDRP activation equilibria, as was pointed out in the recent experimental study of the ATRP equilibrium for the $FeBr_2/FeBr_3$ couple.[62] In principle, the tetradentate diaminobis(phenolato) ligand is unlikely to be displaced by coordinating solvents. However, the coordination sphere may be expanded by additional coordination of a donor molecule for the 5-coordinate **I** and **III** systems and especially for the 4-coordinate **II** system; hence, the values reported in Table 5 should be considered of no great significance when the polymerization is conducted in coordinating solvents. In a noncoordinating solvent, or in bulk monomer, the values may be closer to the reality. Monomer coordination through the π electrons should not take place given the high spin configuration, and no olefin complexes of Fe^{II} or Fe^{III} are known in the presence of unpaired electrons. If solvation may indeed occur, this should in principle affect the less saturated Fe^{II} species to a greater extent. In that case, the transformation of the Fe^{II} system to the Fe^{III} system in ATRP activation and in OMRP deactivation might be associated with an even greater volume increase, further increasing the values shown in the table (more positive V_{ATRP}; more negative V_{OMRP}). The same effect is expected if species **II** dimerizes.

CONCLUSION

The present computational investigation supports the proposition of a dual controlling mechanism via ATRP and OMRP for the polymerization of styrene by complex $\mathbf{I}^{Cl}$.[22,23] The energy change associated with the radical trapping process increases for both the ATRP ($\mathbf{I}^{Me}$ to $\mathbf{I}^{Cl}$) and OMRP ($\mathbf{II}^{Me}$ to $\mathbf{II}^{Cl}$) trapping equilibria. The Cl substituents' electronic inductive effects make it more difficult for the Fe^{II} in **II** to be oxidized to Fe^{III}−Cl, rendering the reverse trapping process in ATRP more favorable. By our calculations, the greater electron withdrawing power of the bis(phenolato) ligand does not negatively affect the formation of the Fe^{III}−alkyl bond in the OMRP dormant species; indeed the latter is slightly more stabilized for the chloro-substituted system $\mathbf{III}^{Cl}$. Geometry and spin state analyses are insensitive to modification of the phenolate substituents, but the small energetic changes are sufficient to affect the delicate activation/deactivation equilibria in a relevant way for polymerization control. The system was further explored by examining the effect of electronic structure on the trapping barriers, suggesting that Fe^{II} systems, in particular, should provide essentially barrier-free ATRP while spin-state factors would be important in the organometallic reaction pathway. This particular system has no trapping barrier because it leads to an intermediate spin organoiron(III) dormant species, but a barrier may be expected for the two-state reaction when the dormant species has a low spin ground state. Finally, pressure as a tool for shaping and understanding controlled radical polymerization reactivity was studied, with preliminary results suggesting model OMRP reactions should be favored at high pressures in noncoordinating solvents. These studies point to the qualitative, not quantitative, mechanistic lessons these computational studies may provide in support of understanding metal-mediated RDRP.

ASSOCIATED CONTENT

Supporting Information

Additional tables of structural parameters and views of optimized structures as described in the text. List of Cartesian coordinates for all optimized structures. This material is available free of charge via the Internet at http://pubs.acs.org.

AUTHOR INFORMATION

Corresponding Author

*Fax: +33-651553003. E-mail: rinaldo.poli@lcc-toulouse.fr.

Author Contributions

The manuscript was written through contributions of all authors. All authors have given approval to the final version of the manuscript.

Notes

The authors declare no competing financial interest.

ACKNOWLEDGMENTS

The authors of this work were granted access to the HPC resources of CINES under allocation 2014-086343 made by GENCI (Grand Equipement National de Calcul Intensif) and to the resources of the CICT (Centre Interuniversitaire de Calcul de Toulouse, project CALMIP). R.P. gratefully acknowledge the Centre National de la Recherche Scientifique (CNRS) and the Institut Universitaire de France (IUF) for additional support. We are grateful to Prof. A. Lledós for helpful discussions.

REFERENCES

(1) Matyjaszewski, K.; Gnanou, Y.; Leibler, L. *Macromolecular Engineering: Precise Synthesis, Materials Properties, Applications*; Wiley-VCH: Verlag GmbH, 2007.

(2) Wang, J.-S.; Matyjaszewski, K. *J. Am. Chem. Soc.* **1995**, *117*, 5614−5615.

(3) Wang, J.-S.; Matyjaszewski, K. *Macromolecules* **1995**, *28*, 7901−7910.

(4) Kato, M.; Kamigaito, M.; Sawamoto, M.; Higashimura, T. *Macromolecules* **1995**, *28*, 1721−1723.

(5) Ando, T.; Kato, M.; Kamigaito, M.; Sawamoto, M. *Macromolecules* **1996**, *29*, 1070−1072.

(6) Ouchi, M.; Terashima, T.; Sawamoto, M. *Chem. Rev.* **2009**, *109*, 4963−5050.

(7) di Lena, F.; Matyjaszewski, K. *Prog. Polym. Sci.* **2010**, *35*, 959−1021.

(8) Matyjaszewski, K.; Jakubowski, W.; Min, K.; Tang, W.; Huang, J. Y.; Braunecker, W. A.; Tsarevsky, N. V. *Proc. Natl. Acad. Sci. U.S.A.* **2006**, *103*, 15309−15314.

(9) Enthaler, S.; Junge, K.; Beller, M. *Angew. Chem. Engl.* **2008**, *47*, 3317−3321.
(10) Ando, T.; Kamigaito, M.; Sawamoto, M. *Macromolecules* **1997**, *30*, 4507−4510.
(11) Poli, R.; Allan, L. E. N.; Shaver, M. P. *Prog. Polym. Sci.*, DOI: 10.1016/j.progpolymsci.2014.06.003.
(12) Gibson, V. C.; O'Reilly, R. K.; Reed, W.; Wass, D. F.; White, A. J. P.; Williams, D. J. *Chem. Commun.* **2002**, 1850−1851.
(13) Gibson, V. C.; O'Reilly, R. K.; Wass, D. F.; White, A. J. P.; Williams, D. J. *Macromolecules* **2003**, *36*, 2591−2593.
(14) Shaver, M. P.; Allan, L. E. N.; Rzepa, H. S.; Gibson, V. C. *Angew. Chem., Int. Ed. Engl.* **2006**, *45*, 1241−1244.
(15) Shaver, M. P.; Allan, L. E. N.; Gibson, V. C. *Organometallics* **2007**, *26*, 4725−4730.
(16) Le Grognec, E.; Claverie, J.; Poli, R. *J. Am. Chem. Soc.* **2001**, *123*, 9513−9524.
(17) Debuigne, A.; Poli, R.; Jérôme, C.; Jérome, R.; Detrembleur, C. *Prog. Polym. Sci.* **2009**, *34*, 211−239.
(18) Smith, K. M.; McNeil, W. S.; Abd-El-Aziz, A. S. *Macromol. Chem. Phys.* **2010**, *211*, 10−16.
(19) Poli, R. In *Polymer Science: A Comprehensive Reference*; Matyjaszewski, K., Möller, M., Eds.; Elsevier BV: Amsterdam, 2012; Vol. 3, p 351−375.
(20) Allan, L. E. N.; Perry, M. R.; Shaver, M. P. *Prog. Polym. Sci.* **2012**, *37*, 127−156.
(21) Poli, R. *Angew. Chem., Int. Ed.* **2006**, *45*, 5058−5070.
(22) Allan, L. E. N.; MacDonald, J. P.; Reckling, A. M.; Kozak, C. M.; Shaver, M. P. *Macromol. Rapid Commun.* **2012**, *33*, 414−418.
(23) Allan, L. E. N.; MacDonald, J. P.; Nichol, G. S.; Shaver, M. P. *Macromolecules* **2014**, *47*, 1249−1257.
(24) Stoffelbach, F.; Poli, R.; Richard, P. *J. Organomet. Chem.* **2002**, *663*, 269−276.
(25) Stoffelbach, F.; Poli, R.; Maria, S.; Richard, P. *J. Organomet. Chem.* **2007**, *692*, 3133−3143.
(26) Champouret, Y.; MacLeod, K. C.; Smith, K. M.; Poli, R. *Organometallics* **2010**, *29*, 3125−3132.
(27) Braunecker, W. A.; Itami, Y.; Matyjaszewski, K. *Macromolecules* **2005**, *38*, 9402−9404.
(28) Braunecker, W. A.; Brown, W. C.; Morelli, B.; Tang, W.; Poli, R.; Matyjaszewski, K. *Macromolecules* **2007**, *40*, 8576−8585.
(29) Frisch, M. J.; Trucks, G. W.; Schlegel, H. B.; Scuseria, G. E.; Robb, M. A.; Cheeseman, J. R.; Scalmani, G.; Barone, V.; Mennucci, B.; Petersson, G. A.; Nakatsuji, H.; Caricato, M.; Li, X.; Hratchian, H. P.; Izmaylov, A. F.; Bloino, J.; Zheng, G.; Sonnenberg, J. L.; Hada, M.; Ehara, M.; Toyota, K.; Fukuda, R.; Hasegawa, J.; Ishida, M.; Nakajima, T.; Honda, Y.; Kitao, O.; Nakai, H.; Vreven, T.; Montgomery, J. A., Jr.; Peralta, J. E.; Ogliaro, F.; Bearpark, M.; Heyd, J. J.; Brothers, E.; Kudin, K. N.; Staroverov, V. N.; Kobayashi, R.; Normand, J.; Raghavachari, K.; Rendell, A.; Burant, J. C.; Iyengar, S. S.; Tomasi, J.; Cossi, M.; Rega, N.; Millam, N. J.; Klene, M.; Knox, J. E.; Cross, J. B.; Bakken, V.; Adamo, C.; Jaramillo, J.; Gomperts, R.; Stratmann, R. E.; Yazyev, O.; Austin, A. J.; Cammi, R.; Pomelli, C.; Ochterski, J. W.; Martin, R. L.; Morokuma, K.; Zakrzewski, V. G.; Voth, G. A.; Salvador, P.; Dannenberg, J. J.; Dapprich, S.; Daniels, A. D.; Farkas, Ö.; Foresman, J. B.; Ortiz, J. V.; Cioslowski, J.; Fox, D. J. *Gaussian 09, Revision C.01*; Gaussian, Inc.: Wallingford, CT, 2009.
(30) Becke, A. D. *J. Chem. Phys.* **1993**, *98*, 5648−5652.
(31) Ehlers, A. W.; Boehme, M.; Dapprich, S.; Gobbi, A.; Hoellwarth, A.; Jonas, V.; Koehler, K. F.; Stegmann, R.; Veldkamp, A.; Frenking, G. *Chem. Phys. Lett.* **1993**, *208*, 111−114.
(32) Grimme, S.; Antony, J.; Ehrlich, S.; Krieg, H. *J. Chem. Phys.* **2010**, 132.
(33) Gütlich, P.; Garcia, Y.; Goodwin, H. A. *Chem. Soc. Rev.* **2000**, *29*, 419−427.
(34) Poli, R. *Chem. Rev.* **1996**, *96*, 2135−2204.
(35) Salomon, O.; Reiher, M.; Hess, B. A. *J. Chem. Phys.* **2002**, *117*, 4729−4737.
(36) Harvey, J.; Aschi, M. *Faraday Discuss.* **2003**, *124*, 129−143.
(37) Harvey, J. N.; Poli, R. *Dalton Trans.* **2003**, 4100−4106.
(38) Carreón-Macedo, J.-L.; Harvey, J. N. *J. Am. Chem. Soc.* **2004**, *126*, 5789−5797.
(39) Besora, M.; Carreon-Macedo, J. L.; Cowan, A. J.; George, M. W.; Harvey, J. N.; Portius, P.; Ronayne, K. L.; Sun, X. Z.; Towrie, M. *J. Am. Chem. Soc.* **2009**, *131*, 3583−3592.
(40) Tabard, A.; Cocolios, P.; Lagrange, G.; Gerardin, R.; Hubsch, J.; Lecomte, C.; Zarembowitch, J.; Guilard, R. *Inorg. Chem.* **1988**, *27*, 110−117.
(41) Velusamy, M.; Palaniandavar, M.; Gopalan, R. S.; Kulkarni, G. U. *Inorg. Chem.* **2003**, *42*, 8283−8293.
(42) Addison, A. W.; Rao, T. N.; Reedijk, J.; Vanrijn, J.; Verschoor, G. C. *J. Chem. Soc., Dalton Trans.* **1984**, 1349−1356.
(43) Allan, L. E. N.; Shaver, M. P.; White, A. J. P.; Gibson, V. C. *Inorg. Chem.* **2007**, *46*, 8963−8970.
(44) Johansson, M. P.; Swart, M. *Dalton Trans.* **2011**, *40*, 8419−8428.
(45) Hirao, H. *J. Phys. Chem. A* **2011**, *115*, 9308−9313.
(46) Siegbahn, P. E. M.; Blomberg, M. R. A.; Chen, S. L. *J. Chem. Theory Comput.* **2010**, *6*, 2040−2044.
(47) Chen, S. L.; Blomberg, M. R. A.; Siegbahn, P. E. M. *J. Phys. Chem. B* **2011**, *115*, 4066−4077.
(48) Carlsson, J.; Aqvist, J. *J. Phys. Chem. B* **2005**, *109*, 6448−6456.
(49) Chang, C. E.; Chen, W.; Gilson, M. K. *J. Chem. Theory Comput.* **2005**, *1*, 1017−1028.
(50) Singh, N.; Warshel, A. *J. Phys. Chem. B* **2009**, *113*, 7372−7382.
(51) Dub, P. A.; Poli, R. *J. Mol. Catal. A* **2010**, *324*, 89−96.
(52) Schwabe, T.; Grimme, S. *Phys. Chem. Chem. Phys.* **2007**, *9*, 3397−3406.
(53) Shaik, S.; Danovich, D.; Fiedler, A.; Schröder, D.; Schwarz, H. *Helv. Chim. Acta* **1995**, *78*, 1393−1407.
(54) Poli, R. In *Comprehensive Inorganic Chemistry II*; Reedijk, J., Poeppelmeier, K., Eds.; Elsevier BV: Amsterdam, 2013; Vol. *9*, pp 481−500.
(55) Harvey, J. N.; Poli, R.; Smith, K. M. *Coord. Chem. Rev.* **2003**, *238*−*239*, 347−361.
(56) Poli, R.; Harvey, J. N. *Chem. Soc. Rev.* **2003**, *32*, 1−8.
(57) Ando, T.; Kamigaito, M.; Sawamoto, M. *Macromolecules* **2000**, *33*, 2819−2824.
(58) Poli, R.; Stoffelbach, F.; Maria, S.; Mata, J. *Chem.—Eur. J.* **2005**, *11*, 2537−2548.
(59) Maria, S.; Stoffelbach, F.; Mata, J.; Daran, J.-C.; Richard, P.; Poli, R. *J. Am. Chem. Soc.* **2005**, *127*, 5946−5956.
(60) Buback, M.; Morick, J. *Macromol. Chem. Phys.* **2010**, *211*, 2154−2161.
(61) Morick, J.; Buback, M.; Matyjaszewski, K. *Macromol. Chem. Phys.* **2011**, *212*, 2423−2428.
(62) Schroeder, H.; Yalalov, D.; Buback, M.; Matyjaszewski, K. *Macromol. Chem. Phys.* **2012**, *213*, 2019−2026.
(63) Buback, M. Personal communication to M.P.S.